ARGONNE NATIONAL LABORATORY
9700 South Cass Avenue
Lemont, Illinois 60439

Origins and optimization of entanglement in plasmonically coupled quantum dots[1]

Matthew Otten, Jeffrey Larson, Misun Min,
Stefan M. Wild, Matthew Pelton, and Stephen K. Gray

Mathematics and Computer Science Division

Preprint ANL/MCS-P5567-0416

April 2016

Updates to this preprint may be found at
http://www.mcs.anl.gov/publications

[1]This material was based upon work supported by the U.S. Department of Energy, Office of Science, Offices of Basic Energy Sciences and Advanced Scientific Computing Research under Contract No. DE-AC02-06CH11357.

Origins and optimization of entanglement in plasmonically coupled quantum dots

Matthew Otten,[1,2] Jeffrey Larson,[2] Misun Min,[2] Stefan M. Wild,[2] Matthew Pelton,[3] and Stephen K. Gray[4]

[1]*Department of Physics, Cornell University, Ithaca, NY 14853*

[2]*Mathematics and Computer Science Division, Argonne National Laboratory, Lemont, IL 60439*

[3]*Department of Physics, University of Maryland, Baltimore County, Baltimore, MD 21250*

[4]*Center for Nanoscale Materials, Argonne National Laboratory, Lemont, IL 60439*

(Dated: April 27, 2016)

Abstract

A system of two or more quantum dots interacting with a dissipative plasmonic nanostructure is investigated in detail by using a cavity and model-Hamiltonian quantum electrodynamics approach. We focus on determining and understanding system configurations that generate multiple bipartite quantum entanglements between the occupation states of the quantum dots. These configurations include allowing for the quantum dots to be asymmetrically coupled to the plasmonic system. Analytical solution of a simplified limit for an arbitrary number of quantum dots and numerical simulations and optimization for the two- and three-dot cases are used to develop guidelines for maximizing the bipartite entanglements. For any number of quantum dots, we show that through simple starting states and parameter guidelines, one quantum dot can be made to share a strong amount of bipartite entanglement with all other quantum dots in the system, while entangling all other pairs to a lesser degree.

PACS numbers: 03.67.Bg,42.50.Dv,42.50.Md,42.50.Pg,73.20.Mf,78.67.Bf

I. INTRODUCTION

Hybrid systems composed of plasmonic nanostructures and quantum emitters/absorbers (e.g., semiconductor quantum dots or other gain media) are currently of much interest. This is due to the plasmonic element's ability to interact strongly with light, leading to subwavelength control and confinement, and the possibility of the quantum element introducing nonlinear optical (as well as more general quantum) responses that may be enhanced by its proximity to the plasmonic element. For example, theoretical predictions of certain Fano resonance phenomena[1–3] in such systems exist, and experiments are approaching the ability to measure such features[4] and have already demonstrated novel lasing action[5] and quantum coherences.[6] The studies of such hybrid systems can also be viewed as steps in the emerging field of "quantum plasmonics,"[7] which aims to realize quantum-controlled devices relevant to quantum sensing, single-photon sources, and nanoscale electronics.

Features relevant to quantum information, such as the entanglement among the quantum dots (QDs), can also be achieved in hybrid plasmonic/QD systems. This ability may seem surprising given the dissipative (or lossy) aspect of plasmonic structures. However, interactions between quantum objects and a dissipative environment lead to the production of stable entangled states.[8–10] Several pioneering theoretical studies have shown that dissipation-induced entanglement is relevant to systems of QDs interacting with plasmonic nanostructures.[11–17]

We previously explored methods for generating entanglement in QD-plasmon systems, using both systems in which only one QD is initially prepared in its excited state and the system evolves without external excitation and systems in which all the QDs are initially in their ground states and the entire system is excited by an ultrafast laser pulse.[18] We showed that either a single or repeated optical pulse entangled the QDs and that the amount of entanglement can be tuned by controlling the coupling of the QDs to the plasmonic nanostructure. Furthermore, the whole system can be excited with a single pulse, without the need to individually address each subsystem. This work and the present work allow for asymmetric coupling of the QDs to the plasmonic system; for example, one can imagine the QDs to be configured to be at different distances from the plasmonic system or in some other way that can lead to asymmetry.

To allow dissipation-induced entanglement to be an effective candidate for quantum in-

formation applications, one must thoroughly understand how the entanglement is generated. Furthermore, constraining parameter sets in experimentally viable regions of the parameter space and knowing the sets' associated degrees of entanglement are important for engineering such systems within any larger quantum information platform. In this paper, we seek to determine system features that maximize the degree of entanglement between the QDs. To accomplish this objective, we employ analysis based on solutions of limiting forms of the problem and optimization based on numerical solutions to the complete cavity quantum electrodynamics equations. We show that for any number of QDs, simple initial conditions and parameter guidelines generate systems where all pairs of QDs share some degree of entanglement.

II. THEORETICAL METHODS

We consider a cavity quantum electrodynamics (CQED) model of a system of N quantum dots in proximity to a plasmonic system. The underlying system's basis states are

$$|q_N, q_{N-1}, \ldots, q_1; s\rangle = |q_N\rangle\, |q_{N-1}\rangle \ldots |q_1\rangle\, |s\rangle\,, \tag{1}$$

where $q_i \in \{\,0, 1\,\}$ represents the exciton of the ith QD and $s \in \{\,0, 1, 2, \ldots, N_s\,\}$ represents the plasmon energy levels. Using a simplified notation $q = q_N, \ldots, q_1$, we can write the density operator as

$$\hat{\rho}(t) = \sum_{qs} \sum_{q's'} C_{qs,q's'}(t)\, |q; s\rangle\, \langle q'; s'|\,. \tag{2}$$

Then our governing equation describing the CQED model is defined as

$$\frac{\mathrm{d}\hat{\rho}}{\mathrm{d}t} = -\frac{i}{\hbar}[\hat{H}, \hat{\rho}] - \frac{i}{\hbar}[\hat{H}_d, \hat{\rho}] + L(\hat{\rho}), \tag{3}$$

where $\hat{H}$, $\hat{H}_d$, and L are the operators for the Hamiltonian, the driving term, and the Lindblad, respectively. The Hamiltonian $\hat{H}$ for the coupled dot-plasmon system as

$$\hat{H} = \sum_i \hat{H}_i + \hat{H}_s + \sum_i \hat{H}_{s,i}. \tag{4}$$

Defining the lowering and raising operator pairs for both the QDs and the plasmon, $(\hat{\sigma}_i, \hat{\sigma}_i^\dagger)$ and $(\hat{b}, \hat{b}^\dagger)$, in the usual manner as in[3,18], we have the isolated dot and plasmon Hamiltonian terms

$$\hat{H}_i = \hbar\omega_i \hat{\sigma}_i^\dagger \hat{\sigma}_i \qquad \text{and} \qquad \hat{H}_s = \hbar\omega_s \hat{b}^\dagger \hat{b}, \tag{5}$$

respectively, and the dot-plasmon coupling terms

$$\hat{H}_{s,i} = -\hbar g_i(\hat{\sigma}_i^\dagger \hat{b} + \hat{\sigma}_i \hat{b}^\dagger). \tag{6}$$

Equation (6) represents the simplest possible dot-plasmon coupling term corresponding to a QD gaining (losing) a quantum of energy when the plasmon loses (gains) a quantum of energy.

For the system exposed to a time-dependent electric field $E(t)$, we have

$$\hat{H}_d = -E(t)\left[\sum_i d_i(\hat{\sigma}_i + \hat{\sigma}_i^\dagger) + d_s(\hat{b} + \hat{b}^\dagger)\right], \tag{7}$$

where d_i and d_s denote the transition dipole moments of the QDs and plasmon, respectively.

We assume that the distance between the QDs is large compared with the separation between QDs and neighboring metal nanoparticles, so that direct through-space coupling among the QDs can be neglected. We also neglect retardation; hence, our treatment is limited to systems with physical dimensions that are small compared with optical wavelengths.

The Lindblad superoperator $L(\hat{\rho})$ in (3) describes the dephasing and dissipation effects. We employ a previously developed[3] extension of $L(\hat{\rho})$ that is parameterized by the QD population decay γ_p, the QD dephasing rate γ_d, and the plasmon decay constant γ_s. We consider time scales on the order of the inverse of these rates, so that there are no correlated fluctuations in the QDs' states and so that the use of the Lindblad superoperator is justified. Although environmental dephasing is explicitly included for the QDs, it is not necessary to do so for the plasmon because the dephasing that arises from its decay (encoded in the corresponding term in $L(\hat{\rho})$) is much larger in magnitude. As in Ref. 3, the rotating wave approximation is applied.

We use Wootter's concurrence[19] to measure the entanglement of the system. An alternative representation of the density operator (2) is the density matrix ρ with its elements defined by

$$\rho_{qs,q's'} = \langle q; s| \hat{\rho} |q'; s'\rangle . \tag{8}$$

Let ρ' be the reduced density matrix associated with one particular pair of QDs, A and B, obtained by tracing the full density matrix ρ over the plasmon quantum numbers s and the quantum numbers for all other QDs. The AB pairwise concurrence is then given by

$$C_{A,B} = \max\{0, \lambda_1 - \lambda_2 - \lambda_3 - \lambda_4\}, \tag{9}$$

where λ_i are the square roots of the eigenvalues of $\rho'\tilde{\rho}'$ with $\lambda_i \geq \lambda_{i+1}$ (in descending order). The matrix $\tilde{\rho}'$ corresponds to the spin-flipped density matrix[19]

$$\tilde{\rho}' = (\sigma_y \otimes \sigma_y)(\rho')^*(\sigma_y \otimes \sigma_y), \tag{10}$$

where

$$(\sigma_y \otimes \sigma_y) = \begin{bmatrix} 0 & 0 & 0 & -1 \\ 0 & 0 & 1 & 0 \\ 0 & 1 & 0 & 0 \\ -1 & 0 & 0 & 0 \end{bmatrix}. \tag{11}$$

A. Approximate Analysis

We define the "dark" evolution to be how a QD-plasmon system evolves given some initial QD excitation with everything else in the system initially in the ground state. In the limit of low total excitation energy one can develop an exact analytical solution for the problem of an arbitrary number of quantum dots interacting with the plasmon if QD dephasing is neglected. This procedure is discussed in Appendix A. We first discuss some predictions from this analysis for two QDs and then briefly for larger numbers of QDs. Also of interest is the case of pulsed excitation, where the system is initially cold and then subjected to a laser pulse. We follow the discussion of the dark evolution with analysis of this pulsed case using simple Rabi flopping ideas.

In the case of two QDs coupled to a plasmon, we are concerned with determining QD-plasmon coupling factors (g_1 and g_2) that maximize entanglement. For two QDs in particular, it is convenient to consider the two entangled QD states

$$|S; s\rangle = \frac{1}{\sqrt{2}}\Big[\, |q_2 = 0\rangle\, |q_1 = 1\rangle + |q_2 = 1\rangle\, |q_1 = 0\rangle \,\Big]\, |s\rangle \tag{12}$$

and

$$|A; s\rangle = \frac{1}{\sqrt{2}}\Big[\, |q_2 = 0\rangle\, |q_1 = 1\rangle - |q_2 = 1\rangle\, |q_1 = 0\rangle \,\Big]\, |s\rangle \tag{13}$$

in our calculations instead of the direct product of primitive QD states as in (1). For two QDs, Appendix A discusses in detail a three-state Hamiltonian model involving the basis states $|0\rangle = |q_2 = 0, q_1 = 0; s = 1\rangle$, $|S\rangle = |S; s = 0\rangle$, and $|A\rangle = |A; s = 0\rangle$ that neglects QD dephasing and spontaneous emission but allows for plasmon dissipation by introducing an

appropriate complex diagonal matrix element to the Hamiltonian matrix. The initial state of relevance to the dark limit calculations is one with an excited QD1, an unexcited QD2, and a plasmon; this state is represented by $|0,1;0\rangle = \frac{1}{\sqrt{2}}(|S\rangle + |A\rangle)$. This initial state is interesting because although it is a separable, unentangled state, it is a nonstationary state of the full system that has been shown to evolve into a state with a possibly significant transient degree of entanglement.[11,12,18] With no plasmon dissipation ($\gamma_s = 0$) and for short times t, the probabilities of states $|0\rangle$, $|S\rangle$, and $|A\rangle$ are given by the respective squares of $a_0(t)$, $a_S(t)$, and $a_A(t)$, where

$$\begin{bmatrix} a_0(t) \\ a_S(t) \\ a_A(t) \end{bmatrix} \approx \begin{bmatrix} -ig_1 t \\ \frac{1}{\sqrt{2}} - \frac{g_1(g_1+g_2)t^2}{2\sqrt{2}} \\ \frac{1}{\sqrt{2}} + \frac{g_1(g_2-g_1)t^2}{2\sqrt{2}} \end{bmatrix}. \tag{14}$$

When $\gamma_s > 0$, the limit as $t \to \infty$ is of interest because the system can then reach a steady state in the populations. Appendix A shows that for the initial condition with one excited QD and the rest of the system unexcited,

$$a_S(\infty) = \frac{1}{\sqrt{2}(1+x^2)} x(1-x) \tag{15}$$

and

$$a_A(\infty) = \frac{1}{\sqrt{2}(1+x^2)} (1-x), \tag{16}$$

where $x = \frac{g_1 - g_2}{g_1 + g_2}$. Remarkably, these results are valid for any positive value of γ_s (although it must be remembered that no QD dephasing has been allowed). The concurrence in this asymptotic limit is simply $|a_A(\infty)|^2 - |a_S(\infty)|^2$ and can be readily maximized to yield the optimum ratio of coupling strengths: $x = -2 + \sqrt{3}$ or

$$\frac{g_2}{g_1} = \sqrt{3}. \tag{17}$$

Appendix A also develops an *exact* procedure for constructing the corresponding dark dynamics of N QDs interacting with a plasmon, without QD dephasing. This system is then described by an effective $(N+1) \times (N+1)$ complex effective Hamiltonian model. For the scenario of one QD initially excited, it can be used to get an idea of how the entanglement results scale with increasing N.

We are also interested in the case when the system is initially unexcited and an optical pulse is used to generate transient entanglement. Assuming the pulse is relatively simple

and resonant with the QDs' transition frequencies, a simple question to ask is what values of g_1 and g_2 will lead to the two-QD system being close to the $|0,1;0\rangle$ state. We know from previous work[11,12,18] that such a system will evolve into a state with some degree of entanglement. On resonance, the QDs undergo Rabi oscillations as they are excited by the laser pulse. The time for QDi to undergo one Rabi oscillation (i.e., to go from the ground state to the excited state and then back to the ground state) is $2\pi/\Omega_R(i)$, where

$$\Omega_R(i) = \frac{\mu_i E_0^{\rm loc}(i)}{\hbar} = \frac{2 g_i \mu_s E_0}{\hbar \gamma_s}, \tag{18}$$

with $E_0^{\rm loc}(i)$ being the amplitude of the sinusoidal electric field experienced locally by QDi. The final term in (18) is obtained by using the expression for $E_0^{\rm loc}$ derived in Appendix B, which relates this local electric field to the incident field E_0. (Other phenomena, such as the Purcell effect, are also occurring; the Rabi formulae (18) discussed here should be construed as approximate indicators of the dynamics.) In order to achieve a highly entangled state, one QD, say QD1, must undergo $m - \frac{1}{2}$ Rabi oscillations (with $m = 1, 2, \ldots$) so that it is left in the excited state. The time for this process to occur is $2\pi(m - \frac{1}{2})/\Omega_R(1)$. The other dot, QD2, must undergo $n = 1, 2, \ldots$ full oscillations so that it is left in its ground state. The time for this process to occur is $2\pi n/\Omega_R(2)$. Equating these two Rabi times leads to the simple result that

$$\frac{g_2}{g_1} = \frac{n}{m - \frac{1}{2}}. \tag{19}$$

We see that the condition (19) on the couplings for achieving one QD excited via pulsed excitation is not the same as the condition (17) on the couplings for that excited state to evolve to an entangled state. Nonetheless, for $m = n = 1$, (19) predicts $g_2/g_1 = 2$, in approximate accord with (17) where $g_2/g_1 \approx 1.73205$. Although this restricts the parameter space for the pulsed case somewhat, many parameters (especially those describing the pulse) can still be varied freely.

B. Concurrence Optimization

To find the set of system parameters that maximize the sum of the pairwise concurrences, we employ a numerical optimization framework that samples the parameter space in a uniformly random fashion, evaluating the concurrence at each point. The parameters in question include the N QD-plasmon coupling coefficients (g_i, $i = 1, 2, \ldots, N$), environmental

aspects such as the QD dephasing and plasmon decay constants (γ_d and γ_s, respectively), and applied laser pulse features such as its fluence (F) and duration (τ). (See Sec. II C for definitions of the laser pulse parameters.) Since the sum of the pairwise concurrences is a nonconvex function of these parameters, several isolated local maxima are likely to exist. Our approach follows that in Ref. 20, clustering evaluated points in the parameter space into basins of attraction for different maxima. Clusters are formed by using the points' function values (sum of pairwise concurrences) and their proximity to points with better function values. Points that do not have a better point within a distance d are considered the best points in their cluster. The distance d can be adjusted so a reasonable number of clusters are identified. (One also can dynamically adjust d as the parameter space is explored.[20,21]) Local optimization runs are then started from the best point in each cluster.

The local optimization problem of maximizing the sum of pairwise concurrences is solved by minimizing the figure of merit

$$\sum_{i<j} \left(1 - C_{i,j}\right)^2 , \tag{20}$$

where $C_{i,j}$ depends on the system parameters being optimized over (see (9)). This form is appropriate because the pairwise concurrences in (20) are bounded above by 1. Depending on the context, $C_{i,j}$ might be the maximum concurrence achieved over time or a long-time asymptotic limit. When viewed as a function of the parameters, (20) defines a nonlinear least-squares problem. We solve this problem with the Practical Optimization Using No Derivatives for sums of Squares (POUNDerS) algorithm.[22,23] For a system with N QDs, POUNDerS iteratively builds local quadratic surrogates of each of the $\binom{N}{2}$ residual functions $\{1 - C_{i,j}\}$ and combines this information in a master surrogate model. In each iteration of the algorithm, this surrogate model is minimized within a trust-region framework to generate candidate solutions.

C. Simulation Details

We consider the time evolution of the density operator in (3), with the choices of the parameters corresponding to a gold nanoparticle system interacting with QDs in a polymer matrix with a dielectric constant $\epsilon_{med} = 2.25$; these choices are similar to those originally used in our single plasmonic-QD system study.[3] For QDi, we choose $\hbar\omega_i = \hbar\omega_s = 2.05$ eV, assuming the QD and plasmon transition energies are equal. We set the QD dipole moments

to be $d_i = 13$ D and the plasmon dipole moment to be $d_s = 4000$ D. The QDs are assumed to have the same spontaneous decay rate, $\hbar\gamma_p = 190$ neV. In some of our calculations we vary or consider several values for the QD dephasing rate, $\hbar\gamma_d$, and plasmon decay rate, $\hbar\gamma_s$. Consistent with our earlier work, base values are $\hbar\gamma_d = 2$ meV and $\hbar\gamma_s = 0.1$ eV. We utilize coupling factors, $\hbar g_i$, in the 0–30 meV range; and unlike all the other QD parameters, we do allow QDs to have different coupling constant values. Previous calculations show that a realistic approximation for the plasmon-QD coupling is approximately 10 meV for a system such as the one we study here.[3] Other systems, such as silver nanoparticles or particles with different geometries, could exhibit larger coupling factors than does gold.[24] For calculations that include a laser pulse $E(t)$, we assume it has the form (in the nonrotating frame) $E(t) = G(t)E_0\cos(\omega_0 t)$, where $\omega_0 = \omega_s = \omega_i$ and $G(t)$ is a Gaussian envelope function such that the full width at half maximum of $E^2(t)$ is τ. The pulse fluence is $F = \int_{-\infty}^{+\infty} dt\sqrt{\epsilon}_{med}c\epsilon_0 E^2(t)$.

We formulate a density matrix equation from (3) using (8), and we solve the density matrix equation consisting of a set of M^2 ordinary differential equations for the time-dependent complex amplitudes $C_{qs,q's'}(t)$, with $M = 2^N N_s$ where N is the number of QDs and N_s is the number of plasmon energy levels. We solve these ODEs numerically using an efficient parallel solver that employs sparse matrix-matrix multiplication algorithms with either a Runge-Kutta or exponential time integration scheme.[25,26]

III. RESULTS

We now detail our quantum dynamics results corresponding to a system of QDs interacting with a plasmonic system as modeled in Sec. II. We analyze such systems for both free evolution of some particular excitation (what we refer to as "dark" evolution) and in the presence of a laser pulse.

A. Two Quantum Dots in the Dark

We first consider two QDs (QD1 and QD2) interacting with a plasmonic system under the assumption that the initial state $|q_2 = 0, q_1 = 1; s = 0\rangle$ has been prepared and evolves in the absence of any external pulses, that is, "in the dark." Unlike cases studied in previous

work,[11,12,18] the possibility of asymmetric dot-plasmon couplings ($g_1 \neq g_2$) can lead to new features in the time-dependent concurrence.

When the QDs are symmetrically distributed within the plasmonic system so that $g_1 = g_2$, the $|A; s\rangle$ state is an eigenstate of the Hamiltonian (4) and decays with a relatively slow dephasing rate (γ_d) due only to the Lindblad term in (3). With finite (but still symmetric) coupling, the $|S; 0\rangle$ state mixes with the $|S; 1\rangle$ state[18] and is no longer an eigenstate of the Hamiltonian. The probability of being in $|S; 0\rangle$ is $\frac{1}{2}\cos^2(\sqrt{2}gt)$, leading to an increased initial decay of the $|S; 0\rangle$ state. The plasmon decay (γ_s) damps out any additional oscillations of the $|S; 0\rangle$ population. As shown previously,[18] starting a system in the $|01; 0\rangle$ state then leads to a high degree of concurrence, since the $|S\rangle$ state quickly decays, while the $|A\rangle$ state undergoes a much slower decay. With $\gamma_d = 0$, the maximum concurrence for such a symmetric system is therefore 0.5. We describe here a method to achieve larger degrees of concurrence by forcing the $|S\rangle$ state to evolve into $|A\rangle$ rather than into $|0, 0\rangle$.

By breaking the symmetry of the couplings between the two QDs, we mix the $|S; 0\rangle$ state with the $|A; 0\rangle$ state, through the $|0, 0; 1\rangle$ state. This approach follows the analysis in Appendix A where a three-state model is discussed and solved analytically in certain limits. When $g_1 = g_2$, no coupling occurs between $|S; 0\rangle$ and $|A; 0\rangle$; but when $g_1 \neq g_2$, the two states are indirectly coupled through the $|0, 0; 1\rangle$ state (to which both states are directly coupled). Starting in the $|0, 1; 0\rangle = (|A; 0\rangle + |S; 0\rangle)/2$ state, and setting $\gamma_s = \gamma_d = 0$ meV, lead to a cyclic evolution between a completely unentangled state and a highly entangled state.

We follow the convention that QD1 is the QD that is initially in its excited state. If $g_1 < g_2$, then the $|A; 0\rangle$ state reaches a population approaching 1 (Fig. 1a); if $g_1 > g_2$, then the $|S; 0\rangle$ state reaches a population approaching 1 (Fig. 1b). The dynamics of these two examples are similar; the $|A; 0\rangle$ (resp. $|S; 0\rangle$) state evolves into the $|0, 0; 1\rangle$ state, which evolves into the $|S; 0\rangle$ (resp. $|A; 0\rangle$) state and back through the $|0, 0; 1\rangle$ state into its initial state. Where the $|S; 0\rangle$ (resp. $|A; 0\rangle$) state reaches its maximum, the concurrence does as well, reaching a value of nearly 1. Using the explicit three-state system described in (A9) in Appendix A, we find the ratio $g_1/g_2 = \sqrt{2} - 1 \approx 0.414$ gives an $|A\rangle$ state population of unity, which also maximizes the concurrence for the $g_1 < g_2$ case. A similar analysis can be done for the $|S\rangle$ state, giving $g_1/g_2 = \sqrt{2} + 1 \approx 2.414$. Note that these optimal ratios for achieving large, instantaneous concurrences when there is no dissipation are different from

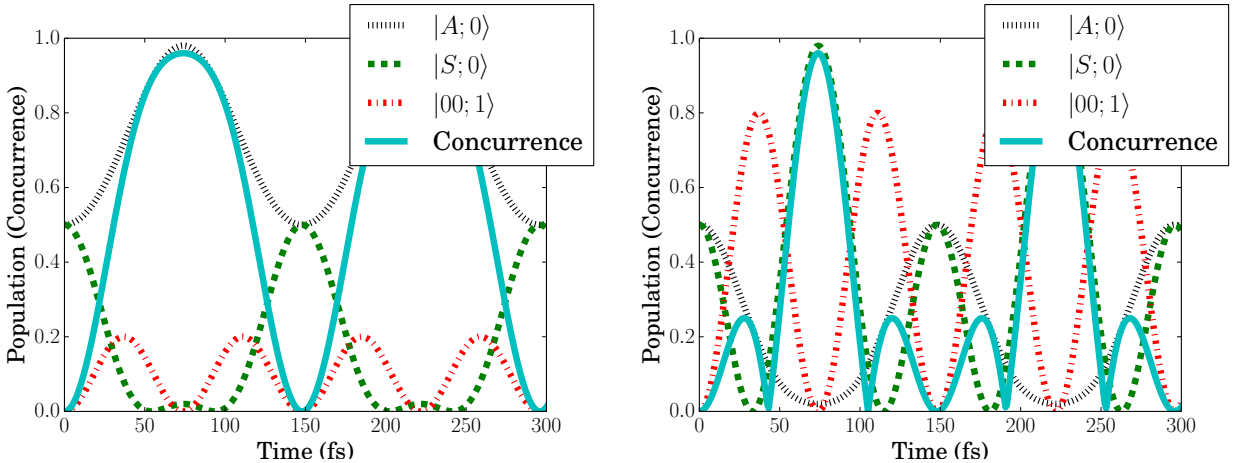

(a) $g_1 = 12.5$ meV, $g_2 = 25$ meV

(b) $g_1 = 25$ meV, $g_2 = 12.5$ meV

FIG. 1: Populations of $|S;0\rangle$, $|A;0\rangle$, $|0,0;1\rangle$, and concurrences for a two-QD system, initially in the $|0,1;0\rangle$ state, with $\gamma_s = \gamma_d = 0$ meV.

those of Sec. II A. The latter concern either an asymptotic concurrence that can be reached in the case of dissipation or the couplings conducive to a pulsed laser generating a particular excited state that can then evolve to a state with significant concurrence.

For short times t, the approximation (14) applies. When $g_1 < g_2$ in this case, the second term of $a_A(t)$ is positive, which leads to a boost in the population of the $|A\rangle$ state. When $g_1 > g_2$, the second term is negative, and the population of the $|A\rangle$ state initially declines. In both cases, $a_S(t)$ initially declines; but when $g_1 > g_2$, it reaches 0 much faster and then rises to nearly 1. Both effects can be seen in Fig. 1.

When the Lindblad terms describing dissipation and dephasing are added, the results of the two simulations $(g_1, g_2) = (12.5$ meV, 25 meV) or (25 meV, 12.5 meV) in Fig. 1 become very different. In Fig. 2 we consider simply adding plasmon dissipation ($\gamma_s > 0$) to the simulations, while keeping the QD dephasing term γ_d at zero. This case also has a closed-form solution (see Appendix A and Sec. II A). We see from Figs. 2(a) and 2(b) that the initial state evolves and begins to populate the first excited plasmon state, but the plasmon population quickly decays and the system reaches a steady state. The steady-state concurrence for the case with $g_1 < g_2$, Fig. 2(a), is larger than the case with $g_1 > g_2$, Fig. 2(b). This trend might be expected on the basis of the dynamics without plasmon decay, Figs. 1(a) and 1(b), wherein a smooth rise of concurrence from 0 to 1 occurs over

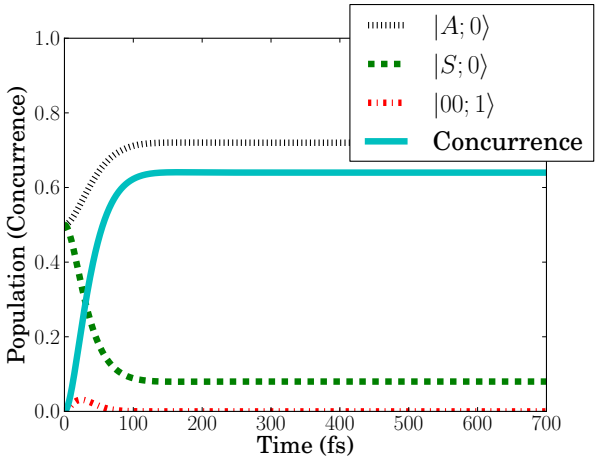

(a) $g_1 = 12.5$ meV, $g_2 = 25$ meV.

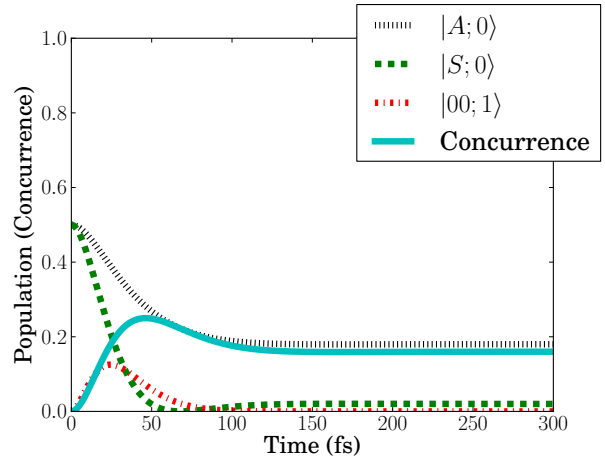

(b) $g_1 = 25$ meV, $g_2 = 12.5$ meV.

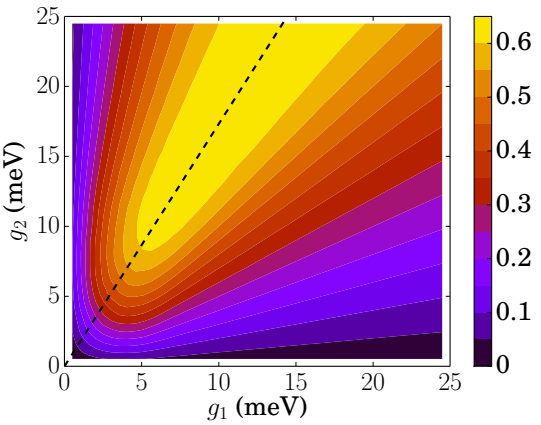

(c) Parameter sweep of many coupling values. The dashed line represents $g_2 = \sqrt{3}g_1$

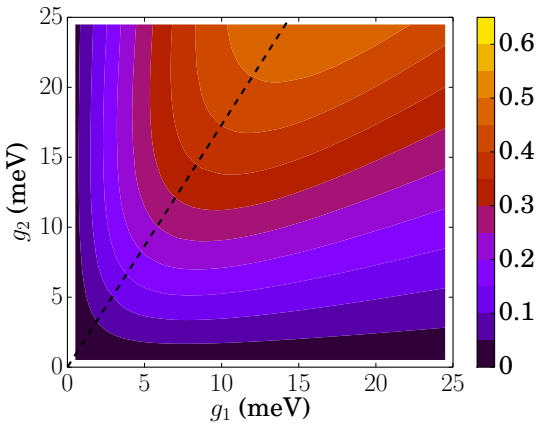

(d) Figure 2(c), but with $\gamma_d = 2.0$ meV.

FIG. 2: Populations of $|S;0\rangle$, $|A;0\rangle$, $|0,0;1\rangle$, and concurrences for a two-QD system, initially in the $|0,1;0\rangle$ state, with $\gamma_s = 100$ meV; (left) $\gamma_d = 0$ meV and (right) $\gamma_d = 2.0$ meV.

initial times for the case $g_1 < g_2$, Fig. 1(a), but a more complicated behavior involving a small local maximum in concurrence occurs for the case $g_1 > g_2$, 1(b). In a realistic system, the $g_1 > g_2$ case will not create concurrences as large as those seen when $g_1 < g_2$; the best case is that the plasmon decay is sufficiently large to stop the $|A;0\rangle$ state from evolving into the $|S;0\rangle$ state. Figure 2(c) shows the maximum concurrence (for each time trajectory) for many different values of g_1 and g_2. There is a clear area of large concurrence when $g_2 \approx \sqrt{3}g_1$ in accordance with the expectation from (17) in Sec. II A. Small discrepancies with respect

to (17) can exist because this equation pertains to the asymptotic concurrence and we are considering the maximum concurrence achieved over a finite window of time.

Note that the isolated QD population decay rates γ_p (discussed in Sec. II C) are sufficiently small and are generally overwhelmed by the Purcell decays that result from finite γ_s and plasmon-dot coupling factors, g_i. Thus, the inclusion of decay in the QD populations has no significant effect on the results presented here for the other parameter values considered. The QD dephasing terms γ_d, however, can have a more significant effect. Figure 2(d) (similar to Fig. 2(c), but with $\gamma_d = 2.0$ meV) shows the maximum concurrence for many values of g_1 and g_2. Naturally, the maximum concurrence is not as large as the $\gamma_d = 0$ meV case. Furthermore, the clear peak around the line $g_2 \approx \sqrt{3}g_1$ has been distorted, although the line still has some significance. Including QD dephasing effects causes the QD populations to decay before significant entanglement can occur, unless the QDs are strongly coupled. At small values of g_i, the optimal point is far from the $\sqrt{3}$ line; but as the couplings are increased, the optimal points again fall upon the $\sqrt{3}$ line. As mentioned above, this derivation pertains to the asymptotic values of the concurrence, but the dephasing does not allow the system to approach that value without larger values of g_i.

B. $N > 2$ Quantum Dots in the Dark

We have used the analytical solution for N QDs interacting with a plasmonic system with no QD dephasing (Appendix A) to explore how the dark entanglement dynamics scales with increasing N beyond $N = 2$. As noted in Sec. III A, introducing dephasing can lead to smaller concurrences and shifts in the optimal g_j/g_i ratios, but our results should indicate what to qualitatively expect as N increases. As in our $N = 2$ dark calculations, the initial condition corresponds to QD1 being initially excited.

For the $N = 3$ case, Fig. 3 shows a contour map of the asymptotic figure of merit (20) as a function of g_2/g_1 and g_3/g_1. The results in this case do not depend on either g_1 or plasmon decay rate γ_s, provided that the latter is positive. (The transient dynamics do depend on both g_1 and γ_s and can also be of interest.) We see that the optimal concurrences are reached at $g_2/g_1 = g_3/g_1 \approx 1.05$, which is somewhat smaller than the $g_2/g_1 = \sqrt{3}$ ratio found for the $N = 2$ case. The optimal values of the concurrence are $C_{1,2} = C_{1,3} \approx 0.450$ and $C_{2,3} = 0.215$. At 0.639, the "direct" concurrence between the excited QD1 and each of

the other $N-1$ dots is slightly smaller than the result for the two-QD system.

Although we have not derived an explicit formula, we can evaluate the exact asymptotic dynamics of the N QD case using the procedure described in Appendix A. We find that for the initial condition in question, two distinct concurrence values always exist: a major one (C^{maj}), associated with all the QD pairs that involve the initially excited QD, and a smaller one (C^{min}), associated with all the indirectly excited pairs. Evaluation of the results for N up to $N = 150$ shows that $C^{\mathrm{maj}} \approx 0.54/\sqrt{N}$, for $N > 100$; that is, the major concurrence tends to zero, although it does so slowly, with an increasing number of QDs. In this limit, the minor concurrence decays somewhat faster, with $C^{\mathrm{min}} \approx 0.50/N$. Also, the optimal concurrence figure of merit is achieved with just one unique ratio for all the couplings, $g_{i>1}/g_1 = x$. We find that $x \approx 1.09/\sqrt{N}$ for $N > 100$.

The optimal value of g_2 becomes less than g_1 when $N = 4$, in contrast to the two- and three-QD systems, where $g_1 > g_2$. This can be explained by looking at the relative fraction of QD pairs, $2/N$, which have $C_{i,j} = C^{\mathrm{maj}}$. When $N < 4$, the fraction of QD pairs that have $C_{i,j} = C^{\mathrm{maj}}$ is greater than $1/2$. As N becomes larger, more and more QD pairs have $C_{i,j} = C^{\mathrm{min}}$. When $g_1 > g_2$, there is a boost in C^{maj}, possibly at the cost of C^{min}. When N is large, the solution from minimizing the figure of merit (20) no longer favors boosting C^{maj}; instead it increases the (more numerous) C^{min}.

The state created by this mechanism, where all QDs share bipartite entanglement (possibly weakly) with all other QDs, is similar to a generalized W-state[27]. In the W-state, all pairs of qubits have the same value of concurrence, and that value is as large as possible. Thus, the W-state is the optimal state, given our figure of merit. According to an idea known as the monogamy of entanglement,[28] there is an upper bound on the possible sum of bipartite entanglement. When $N > 2$, each qubit pair can no longer be fully entangled. As N increases, the maximum bipartite concurrence for each pair in the W-state decreases as $2/N$. This represents a fundamental limit on the entanglement that we can achieve in our system. The decay of the concurrence with increasing N in our QD-plasmon system is similar to that of the W-state. Furthermore, if we measure the initially excited QD, we can project onto a state where QD pairs share a small degree of entanglement with each other. Taking a ratio of the asymptotic value of C^{min} in the projected state to the W-state concurrence shows that each QD pair will have only $1/4$ of the concurrence of the W-state. While this may be a small fraction, it is a constant fraction with increasing N, allowing a

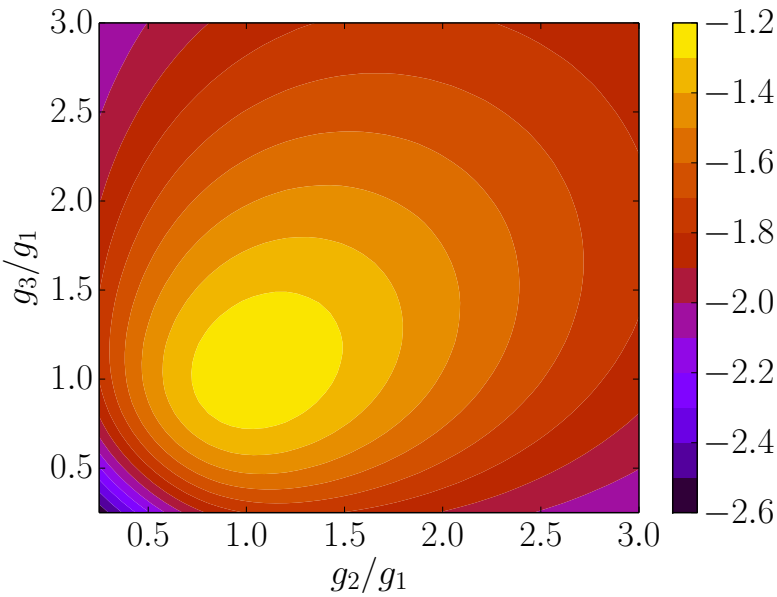

FIG. 3: Asymptotic figure of merit (20) for 3 QDs, with one QD initially excited, $\gamma_s > 0$, and $\gamma_d = 0$, as a function of the ratios of the coupling parameters.

(low-fidelity) approximate W-state to be easily created for any number of QDs. The addition of decay in the QD populations will further decrease the fidelity; but, as shown in the two-QD case, the entanglement still persists, although at a smaller value.

C. Two Quantum Dots Subjected to Ultrafast Laser Pulses

Preparing a system in the initial state $|0, 1; 0\rangle$ can create high degrees of entanglement, but it does not represent a simple experimental setup. A simpler setup is to prepare a system and excite it with a single optical pulse. Introducing a laser pulse to a system increases the number of parameters that the system depends on and can have a large effect on the value of the concurrence.[18] For the two-QD system, the parameters varied include the laser fluence (F), laser duration (τ), coupling strengths (g_1 and g_2), QD dephasing (γ_d), and plasmon dephasing (γ_s); ω_i, ω_s, d_i, d_s, and γ_p remain fixed. We also constrained the parameter values in a physically reasonable part of the parameter space; see Table I.

We used POUNDerS to find optimal parameters in different parts of the parameter space defined in Table I. We optimized the sum of the maximum value of the pairwise concurrence over the time horizon; other figures of merit (such as the sum of the integral of the pairwise

TABLE I: Constraints for optimization parameters.

Parameter	**Lower Bound**	**Upper Bound**
g_i (meV)	0	25
F (nJ/cm^2)	0	700
τ (fs)	10	200
γ_d (meV)	0	5
γ_s (meV)	100	300

concurrences over the time window) will be investigated in future work.

The evolution of the pairwise concurrence and the states' populations for a locally optimal result is plotted in Fig. 4(a) and is shown to behave similarly to the system with one initially excited QD shown in Fig. 2(a). In contrast to that system, the plasmon population (not plotted) reaches a much higher value of nearly 10 in this system. We previously discovered that we had to allow g_1 and g_2 to differ in order to create large amounts of concurrence because doing so allowed the system to approximate the $|0,1\rangle$ state, creating a highly entangled state, with the proper parameter choices.[18] We noted there that the less-strongly coupled QD achieved a higher population after the pulse concluded. The boost in the $|A;s=0\rangle$ population we describe in this paper for the case $g_1 < g_2$ (see discussion of Fig. 1) is also present, helping raise the concurrence higher and thereby allowing the pulsed case to reach levels of concurrence similar to those for the dark case. This is clearly seen in Fig. 4(b). After the pulse ends, the $|S;0\rangle$ state begins to decline, but the $|A;0\rangle$ state grows, because of their indirect coupling. This boost of the $|A;0\rangle$ state is the same as seen in the dark case. Figures 4(c)–4(d) also show this same parameter set with larger values of γ_d. The maximum value of the pairwise concurrence strongly depends on the QD dephasing, γ_d. This dependence is not surprising, because longer coherence times are almost always associated with larger degrees of (and longer-lived) entanglement. Figure 4(c) shows the system at $\gamma_d = 0.2$ meV (approximately liquid helium temperatures), while Fig. 4(d) shows the system at $\gamma_d = 2.0$ meV (approximately liquid nitrogen temperatures). The loss in concurrence from $\gamma_d = 0$ meV to $\gamma_d = 0.2$ meV is only about 10%, but it is almost 50% when γ_d is raised to 2.0 meV. Generally, the concurrence increases with decreasing γ_d.

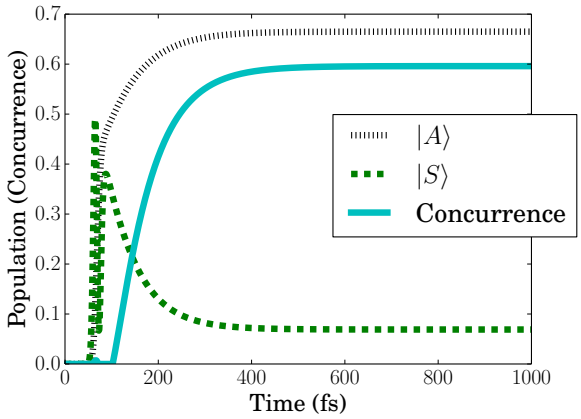

(a) $\gamma_d = 0$ meV; locally optimal result.

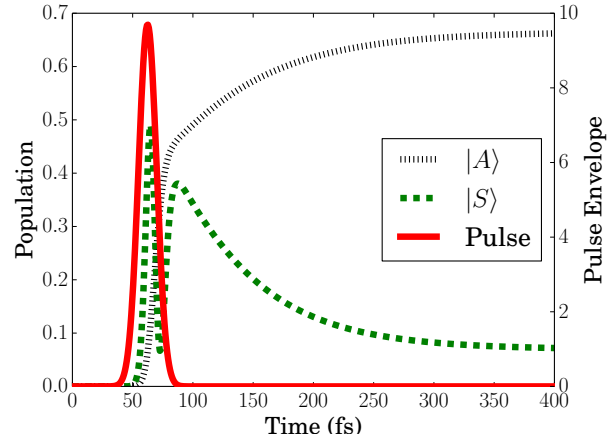

(b) $\gamma_d = 0$ meV; locally optimal result, with pulse envelope.

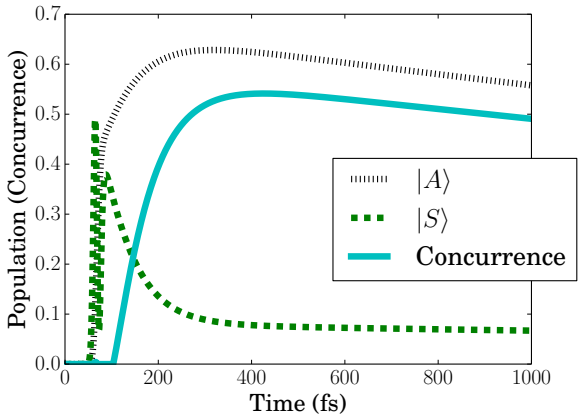

(c) $\gamma_d = 0.2$ meV.

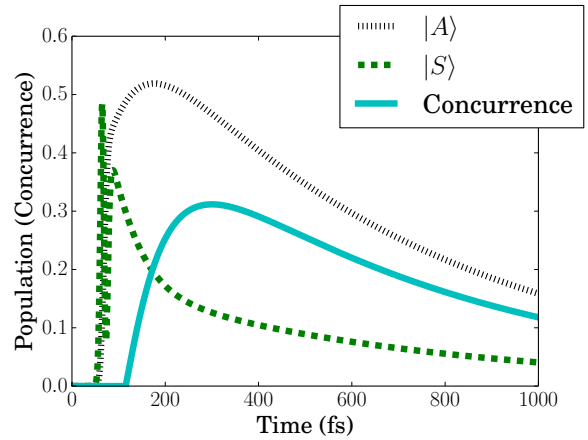

(d) $\gamma_d = 2.0$ meV.

FIG. 4: Populations of $|A\rangle$ and $|S\rangle$ and concurrences for the final parameters from a local optimization run on the two-QD system. The final parameters are $g_1 = 12.8$ meV, $g_2 = 24.9$ meV, $F = 263.4$ nJ/cm^2, $\tau = 12.5$ fs, $\gamma_s = 186$ meV, and $\gamma_d = 0$ meV. Figures 4(c)–4(d) change only γ_d, while leaving all other parameters the same.

Figure 5 shows the maximum concurrence over our time window as g_1 and F vary, for fixed pulse duration (τ) and coupling strength of the second QD (g_2). An interesting consequence of the Rabi oscillations is bifurcations of the areas of high concurrence. At small laser fluences, given $g_1 < g_2$, there is only one region of high concurrence corresponding to one QD undergoing a half Rabi oscillation and the other undergoing one oscillation; that is, the $m = n = 1$ case from Sec. II A that was predicted to maximize entanglement. As the

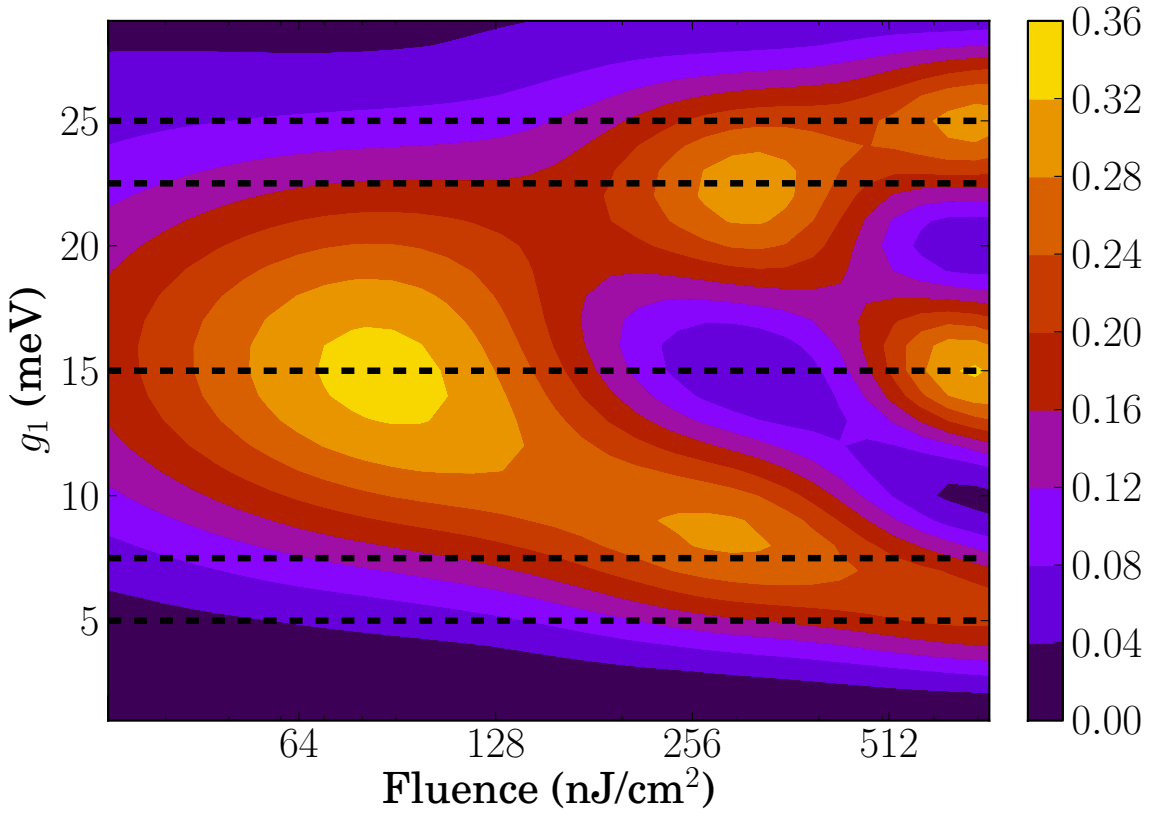

FIG. 5: Maximum concurrence for a parameter sweep of the two-QD system, with $g_2 = 30$ meV, $\tau = 20$ fs, $\gamma_s = 150$ meV, $\gamma_d = 2$ meV. The dashed lines represent coupling ratios obeying (19).

laser fluence is increased, the region of high concurrence splits into two regions, as the more-strongly coupled QD approaches two full Rabi oscillations. The less-strongly coupled QD can now either go through half or three-halves Rabi oscillations to end up in the excited state. This region bifurcates again, as the second dot approaches three Rabi oscillations. This analysis works for the two-QD and three-QD systems we present in this paper, but it gives a relationship only between two of the parameters, g_1 and g_2. Since we have many other parameters to optimize over, POUNDerS is used to find local optima of the maximum concurrence.

D. Three Quantum Dots Subjected to Ultrafast Laser Pulses

Since the QDs are assumed to be coupled to the plasmon but not to each other, adding a QD increases the number of parameters only by one (g_3, the new QD's coupling to the plasmon). More importantly, the size of the Hilbert space needed for the simulation increases by a factor of 2, more than quadrupling the simulation's run time and making the optimization algorithm's ability to quickly find locally optimal solutions even more important. Here we present two locally optimal points for a three-QD system. The QD dephasing, γ_d, is fixed to 0.2 meV, since this approximates a physically realizable system at liquid helium temperatures.

Figure 6 shows the populations of the QDs and their pairwise concurrences for the system parameters returned from a local optimization run. This system is analogous to the two-QD systems discussed above, since $g_2 = g_3$. QD2 and QD3 undergo two Rabi flops, and QD1 undergoes one-and-a-half Rabi flops. Accordingly, $g_2/g_1 = g_3/g_1 = 1.322 \approx \frac{4}{3}$, as predicted by (19). The boost of the population of the $|A;0\rangle$ state is also apparent in this system. Shortly after the pulse has concluded, the $|A;0\rangle$ state is still rising, while the $|S;0\rangle$ state decays. The boost of the $|A;0\rangle$ state eventually finishes and the $|S;0\rangle$ and $|A;0\rangle$ states then decay at similar rates. Aside from having a much larger concurrence than presented previously, the pulsed three QD simulations presented in this paper are also interesting because their coupling parameters are smaller and represent a more physically reasonable system than do our previous results.[18]

Figure 7 shows the populations and concurrences for a system with the best parameters from a different local optimization run. The QDs in this system all have different coupling values (as opposed to the previous example where $g_2 = g_3$), leading to three different pairwise concurrences, even though the populations of QD2 and QD3 are similar in value. QD3 undergoes four Rabi flops, while QD1 undergoes three-and-one-half Rabi flops, leading to $g_3/g_1 = 1.142 \approx \frac{8}{7}$. Additionally, QD2 undergoes three Rabi flops, leading to $g_2/g_1 = 0.858 \approx \frac{6}{7}$. Both these pairs agree with (19). The QD3:QD1 subsystem, where the excited QD has a smaller coupling value, exhibits the boost of the population of the $|A;0\rangle$ state described previously, as shown in Fig. **??**(c). Contrast this with the QD2:QD1 subsystem, Fig. **??**(d), which does not experience the boost, since the excited QD has a larger coupling. After the pulse concludes, the $|S;0\rangle$ state undergoes a similar evolution, but the $|A;0\rangle$ state is

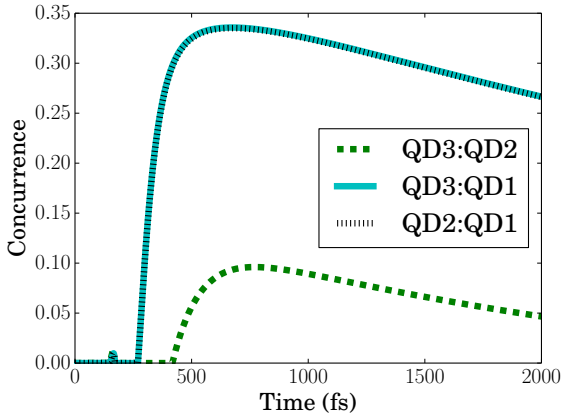

(a) Concurrences for all three subsystems.

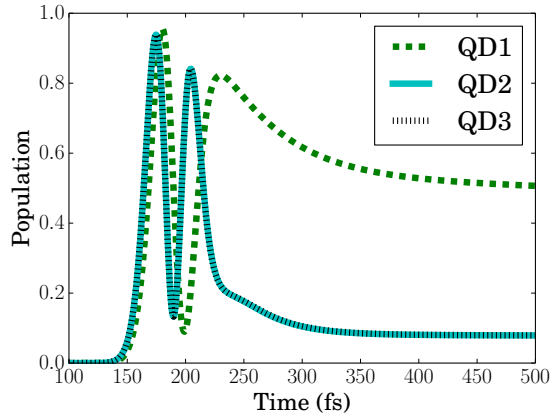

(b) Quantum dot populations.

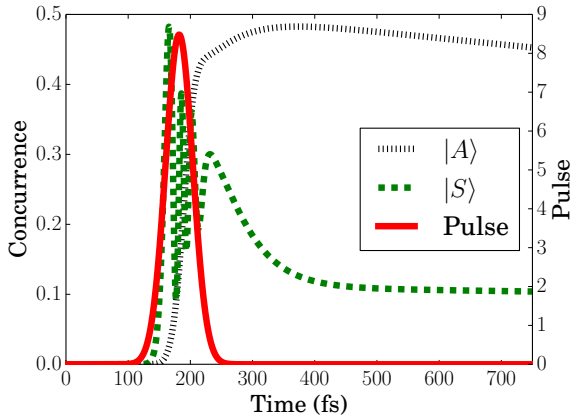

(c) $|S;0\rangle$ and $|A;0\rangle$ states and pulse for the QD3:QD2 and QD3:QD1 subsystems.

FIG. 6: Populations and concurrences for the final parameters from a local optimization run on the three-QD system with γ_d fixed at 0.2 meV. The final parameters are $g_1 = 14.6$ meV, $g_2 = 19.3$ meV, $g_3 = 19.3$ meV, $F = 587.0$ nJ/cm^2, $\tau = 36.4$ fs, and $\gamma_s = 180.4$ meV (with γ_d fixed at 0.2 meV).

different. In the QD3:QD1 subsystem the $|A;0\rangle$ state increases after the pulse has concluded, but in the QD2:QD1 subsystem the $|A;0\rangle$ state only decreases. As a result, the QD3:QD1 concurrence ends up greater than the QD2:QD1 state, even though the populations of QD2 and QD3 end up at similar values.

We note that the Rabi-flop mechanism of (19) singles out one QD (the one undergoing $m-\frac{1}{2}$ Rabi flops) to become strongly entangled with all other QDs, while the other two QDs

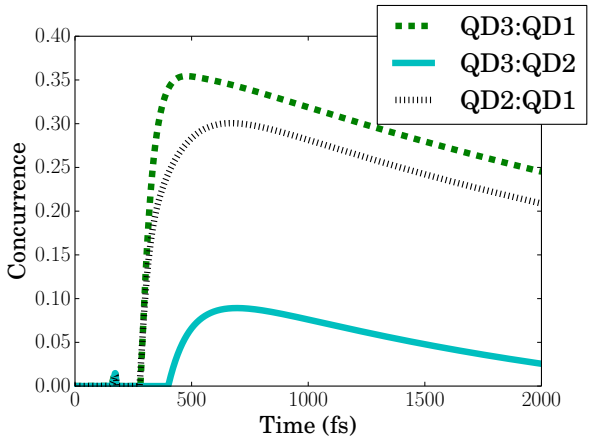

(a) Concurrences for all three subsystems.

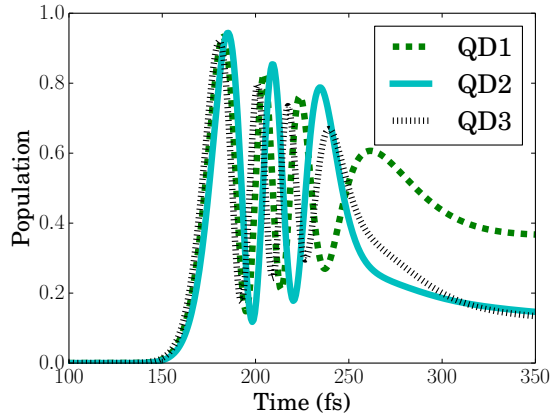

(b) Quantum dot populations.

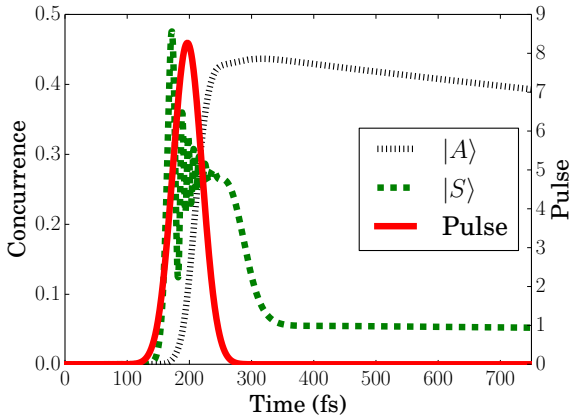

(c) $|S;0\rangle$ and $|A;0\rangle$ states and pulse for the QD3:QD1 subsystem.

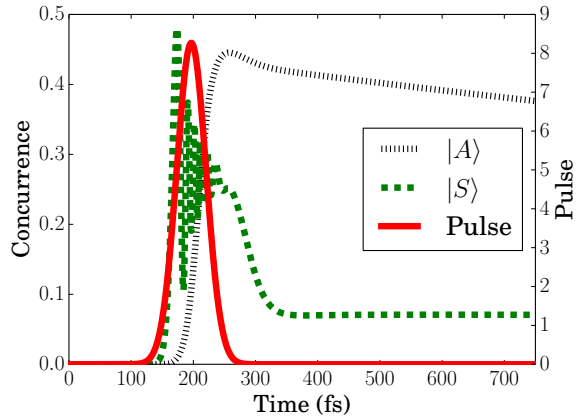

(d) $|S;0\rangle$ and $|A;0\rangle$ states and pulse for the QD2:QD1 subsystem.

FIG. 7: Populations and concurrences for the final parameters from a second local optimization run on the three-QD system with γ_d fixed at 0.2 meV. The final parameters are $g_1 = 19.0$ meV, $g_2 = 16.3$ meV, $g_3 = 21.7$ meV, $F = 603.4$ nJ/cm^2, $\tau = 39.4$ fs, and $\gamma_s = 107.7$ meV (with γ_d fixed at 0.2 meV).

become strongly entangled only with the excited QD and become weakly entangled with each other. This is an inherent limit of the prescription described. Remarkably, entanglement between the two approximate ground state QDs reaches the level that it does, even for identical QDs (i.e., a concurrence of 0.1 in Fig. 6), but the entanglement is still much smaller than the entanglement they share with the excited QD. Since the pulse approximately prepares the same state studied in Sec. III B and the Rabi-flop mechanism can be used for

TABLE II: Summary of optimization run results for a laser pulse interacting with a system composed of two and three quantum dots. An "^{f}" denotes that the parameter value was fixed and therefore not optimized over.

	Two QDs	**Three QDs, Solution 1**	**Three QDs, Solution 2**
g_1 (meV)	12.8	14.6	19.0
g_2 (meV)	24.9	19.3	16.3
g_3 (meV)	—	19.3	21.7
F (nJ/cm^2)	263.4	587.0	603.4
τ (fs)	12.5	36.4	39.4
γ_d (meV)	0	0.2^f	0.2^f
γ_s (meV)	186	180	108
Figure	Fig. 4	Fig. 6	Fig. 7
Maximum bipartite concurrence	0.60	0.34	0.35

N quantum dots, we can again project onto a (low-fidelity) approximate W-state, where all pairs of QDs share the same amount of bipartite entanglement. This approach could be more experimentally feasible than having a previously excited QD, but the bipartite concurrence values will be lower than those of Sec. III B.

IV. CONCLUDING REMARKS

We provide a detailed explanation of the origins and optimization of bipartite (or pairwise) entanglement in two, three, and an arbitrary number of QDs coupled to a plasmonic system. We analyze systems with an initially excited state as well as initially unexcited systems excited by a laser pulse. We vary the QD-plasmon coupling values (which represent a QD's distance from the plasmonic system), as well the femtosecond pulse parameters and dephasing rates to explore entanglement generation. By utilizing the full density matrix master equation, we are able to study the entanglement (via concurrence) of many different systems.

In the case of two QDs, two mechanisms are identified as the source of the entanglement

generation: the differing decay rates of the $|S;0\rangle$ and $|A;0\rangle$ states (previously identified)[18] and a new mechanism involving an indirect coupling between the $|S;0\rangle$ and $|A;0\rangle$ states that leads to a boost in the $|A;0\rangle$ state population. With no dephasing or decay, high degrees of entanglement can be generated by having near-unity populations of either the $|A;0\rangle$ or $|S;0\rangle$ states. When plasmon decay is added, however, the entanglement generated from $|A;0\rangle$ is much higher than that of $|S;0\rangle$. A simple analysis including plasmon decay but neglecting QD dephasing predicts that the asymptotic concurrence is maximized when $g_2/g_1 = \sqrt{3}$ in the dark case; calculations show that this relation is still useful when QD dephasing is considered.

The two entanglement-generating mechanisms are most apparent when the system is initially prepared with equal amounts of $|S;0\rangle$ and $|A;0\rangle$, which is most easily achieved by having one excited QD and the other QD in the ground state. This dark case may be contrasted with attempts to generate entanglement in initially unexcited systems by using laser pulses. On the basis of optimization, we find that only certain sets of parameters generate an analog to the dark case. In particular, certain rational values of the ratio of the QD-plasmon couplings, g_i/g_j, lead to results comparable to the dark case. These ratios can be understood by analyzing the underlying Rabi flops of the component QDs; the target final state, after the pulse, consists of one QD excited and the other QD in the ground state. To achieve this, one QD undergoes $m - \frac{1}{2}$ Rabi oscillations, leaving it in an approximate excited state, while the other QD undergoes n full oscillations, leaving it in an approximate ground state. This method will work for any pair of QDs, even if that pair is part of a larger system of N QDs.

In the case of three QDs, we optimize the sum of the bipartite concurrences among all of the pairs. Several local maxima corresponding to different sets of system parameters are obtained, and we present two in this paper. One ("solution 1") was analogous to the two-QD systems discussed above, with $g_1 < g_2 = g_3$, while the other ("solution 2") had $g_2 < g_1 < g_3$; both exhibited the entanglement generation mechanisms described above. The parameters for all three optimal systems are listed in Table II. The ratios of the g_i values in the highly entangled pairs of these three-QD systems follow the simple rules derived from the Rabi-flop analysis.

We also extended our results to N QDs, with some simplifying assumptions, such as no QD population decay and a single initially excited QD. For any number of QDs, all pairs

of QDs will become entangled. However, since this mechanism relies on one QD being in the excited state and the rest of the QDs being in the ground state, these mechanisms can strongly entangle only a fraction $(2/N)$ of the pairs of QDs. Using the simple rules laid out in this paper for a large number of QDs results in the excited QD being strongly entangled with all other QDs, but all the ground state QDs will be strongly entangled only with the excited QD and only weakly entangled with each other. Since all QDs share some amount of bipartite entanglement with all other QDs, the resulting state is similar to a generalized W-state and, with a measurement of the excited QD, can be projected to a state where all pairs of QDs share the same amount of bipartite concurrence (though this projected state only has 1/4 of the bipartite concurrence of a true W-state).

Additionally, this procedure could generate certain types of cluster states. A cluster state is a graph in which qubits are represented by nodes on a graph, and an edge between two nodes represents entanglement between the two qubits.[29] The W-state would be a cluster state represented by a complete, fully connected graph. An important subclass of cluster states is the star state, where a central node is connected to all other nodes (or, a single qubit is entangled to all other qubits but the other qubits are not entangled with each other). A four-qubit star cluster can be used for universal quantum computing.[30] In our model, we have an approximate star cluster for N QDs, since the initially excited QD is strongly entangled with all other QDs. Although we showed N QD results only for a specific initial starting condition, we also show how this state can be prepared for N QDs from a single, ultrafast laser pulse. The rules for the ratios of the coupling strengths based on the number of Rabi flops can be used to define an appropriate set of parameters to prepare an approximate form of the specific initial starting condition studied.

Further studies of such systems that better approximate the W-state are planned, as are studies of the entanglement between all qubits of the system (rather than just pairs), which would be similar to the GHZ-state,[27] which represents entanglement where all of the qubits are mutually entangled with each other (rather than just sharing bipartite entanglement with other qubits). The W- and GHZ-states represent two mutually exclusive examples of multipartite entanglements and allow entanglement to be used as a quantum information resource in different ways.[27] We will also apply the same ideas and methods to other systems, such as nitrogen vacancies in diamond and superconducting qubits.

Acknowledgments

This work was performed at the Center for Nanoscale Materials, a U.S. Department of Energy, Office of Science, Office of Basic Energy Sciences User Facility and supported by the U.S. Department of Energy, Office of Science, Office of Advanced Scientific Computing Research (both under Contract No. DE-AC02-06CH11357). We thank Ron Shepard for helpful suggestions concerning some of the analytical analysis presented in this paper. We thank Todd Pittman and Jason Kestner for helpful discussions.

Appendix A: Three and $N+1$ State Models

The "dark" problem, namely, to determine the dynamics of N QDs and a plasmonic system that results from a given initial condition without any applied laser pulse, can be solved analytically if the initial condition is not too energetic and QD dephasing is neglected. An example of such a system would be if there is just one quantum of excitation within the QD manifold and a cold plasmonic system. The analytical solution is made possible because under such conditions a time-dependent Schrödinger equation involving an effective, non-Hermitian Hamiltonian can be employed and the latter can be represented by an $(N+1)\times(N+1)$ matrix with a simple structure. First we illustrate such a solution in detail for the case of $N=2$. We then present the general $N+1$ state solution.

For two QDs interacting with a plasmonic system, we wish to solve for the time evolution of $|\Psi(t)\rangle$ satisfying

$$i\hbar\frac{\partial}{\partial t}|\Psi(t)\rangle = \hat{H}|\Psi(t)\rangle\,, \tag{A1}$$

where

$$\begin{aligned}|\Psi(t)\rangle = \; & c_0(t)\,|q_2=0,q_1=0;s=1\rangle \\ & + c_S(t)\,|S;s=0\rangle + c_A(t)\,|A;s=0\rangle\,.\end{aligned} \tag{A2}$$

We refer to the three states $|q_2=0,q_1=0;s=1\rangle$, $|S;s=0\rangle$, and $|A;s=0\rangle$ as the zero-order basis. This limited basis is adequate for describing an initial condition that involves any superposition of these three states, such as the case of one QD being excited and the plasmonic system and other QD being cold. For brevity, we will sometimes use the condensed notation for the three zero-order basis states $|0\rangle = |q_2=0,q_1=0;s=1\rangle$, $|S\rangle = |S;s=0\rangle$, and $|A\rangle = |A;s=0\rangle$. With the definitions of the basis states in the text, (1), (12), and

(13), and the Hamiltonian operator, (4), the corresponding 3×3 Hamiltonian matrix of the zero-order basis representation is

$$\boldsymbol{H} = \hbar \begin{bmatrix} \omega_0 & \alpha & \beta \\ \alpha & \omega_0 - i\epsilon & 0 \\ \beta & 0 & \omega_0 \end{bmatrix}. \tag{A3}$$

The QD and plasmon transition frequencies are assumed to be equal, $\omega_1 = \omega_2 = \omega_s$, the coupling between $|0,0;1\rangle$ and $|S;0\rangle$ is

$$\alpha = \frac{1}{\sqrt{2}}\big(g_1 + g_2\big), \tag{A4}$$

and the coupling between $|0,0;1\rangle$ and $|A;0\rangle$ is

$$\beta = \frac{1}{\sqrt{2}}\big(g_1 - g_2\big). \tag{A5}$$

We assume no direct coupling between $|S;0\rangle$ and $|A;0\rangle$. Notice that in (A3), we have added an imaginary part $-i\epsilon$ to the diagonal matrix element associated with $|0,0;1\rangle$. With $\epsilon = \gamma_s/2$ this term represents the dissipative loss of the plasmonic system.

Introducing the more slowly varying coefficient vector

$$\begin{bmatrix} a_0(t) \\ a_S(t) \\ a_A(t) \end{bmatrix} = \exp\left(i\omega_0 t\right) \begin{bmatrix} c_0(t) \\ c_S(t) \\ c_A(t) \end{bmatrix}, \tag{A6}$$

(A1) leads to

$$\frac{d}{dt} \begin{bmatrix} a_0(t) \\ a_S(t) \\ a_A(t) \end{bmatrix} = -i\boldsymbol{W} \begin{bmatrix} a_0(t) \\ a_S(t) \\ a_A(t) \end{bmatrix}, \tag{A7}$$

where

$$\boldsymbol{W} = \begin{bmatrix} 0 & \alpha & \beta \\ \alpha & 0 & 0 \\ \beta & 0 & 0 \end{bmatrix}. \tag{A8}$$

The solution of (A7) is thus

$$\begin{bmatrix} a_0(t) \\ a_S(t) \\ a_A(t) \end{bmatrix} = \exp\left(-i\boldsymbol{W}t\right) \begin{bmatrix} a_0(0) \\ a_S(0) \\ a_A(0) \end{bmatrix}. \tag{A9}$$

In the limit (assuming no plasmon dissipation, $\epsilon = 0$), expanding the exponential and re-grouping terms, (A9) can be written more explicitly as

$$\begin{bmatrix} a_0(t) \\ a_S(t) \\ a_A(t) \end{bmatrix} = \begin{bmatrix} a_0(0) \\ a_S(0) \\ a_A(0) \end{bmatrix} + \left(\begin{bmatrix} \eta^2 & 0 & 0 \\ 0 & \alpha^2 & \alpha\beta \\ 0 & \alpha\beta & \beta^2 \end{bmatrix} \frac{F(t)}{\eta^2} - i\boldsymbol{W}\frac{G(t)}{\eta} \right) \begin{bmatrix} a_0(0) \\ a_S(0) \\ a_A(0) \end{bmatrix}, \tag{A10}$$

where

$$\eta = \sqrt{\alpha^2 + \beta^2} \tag{A11}$$

and

$$F(t) = \cos(\eta t) - 1, \quad G(t) = \sin(\eta t). \tag{A12}$$

Note that for the initial condition corresponding to $|\Psi(t=0)\rangle = |q_2 = 0, q_1 = 0; s = 0\rangle$ or $a_0(0) = 0$, $a_S(0) = a_A(0) = \frac{1}{\sqrt{2}}$, the above exact solution (for $\epsilon = 0$) is such that $a_0(t)$ is a purely imaginary number for all times and that $a_S(t)$ and $a_A(t)$ are purely real numbers for all times. Equation (A10), can be approximated to various orders in time by expanding $F(t)$ and $G(t)$ defined in (A12) appropriately. Thus, with the initial condition $|\Psi(t=0)\rangle = |q_2 = 0, q_1 = 1; s = 0\rangle$, the approximate solution, accurate to second order in time, is

$$\begin{bmatrix} a_0(t) \\ a_S(t) \\ a_A(t) \end{bmatrix} \approx \begin{bmatrix} -i\frac{(\alpha+\beta)t}{\sqrt{2}} \\ \frac{1}{\sqrt{2}} - \frac{(\alpha^2+\alpha\beta)t^2}{2\sqrt{2}} \\ \frac{1}{\sqrt{2}} - \frac{(\beta^2+\alpha\beta)t^2}{2\sqrt{2}} \end{bmatrix}, \tag{A13}$$

or, in terms of g_1 and g_2,

$$\begin{bmatrix} a_0(t) \\ a_S(t) \\ a_A(t) \end{bmatrix} \approx \begin{bmatrix} -ig_1 t \\ \frac{1}{\sqrt{2}} - \frac{g_1(g_1+g_2)t^2}{2\sqrt{2}} \\ \frac{1}{\sqrt{2}} + \frac{g_1(g_2-g_1)t^2}{2\sqrt{2}} \end{bmatrix}. \tag{A14}$$

Of course, another way to obtain (A10) is to determine the eigenvalues and eigenvectors of $\hat{W}$, w_k and $|\phi_k\rangle$, $k = 1, 2, 3$, and represent (A9) with them. This procedure can be carried out exactly even when plasmonic dissipation is allowed ($\epsilon > 0$). The eigenvalues of $\boldsymbol{W}$ are

easily found to be

$$\begin{aligned} w_1 &= 0 \\ w_2 &= \frac{1}{2}(-i\epsilon - \sqrt{4\alpha^2 + 4\beta^2 - \epsilon^2}) \\ w_3 &= \frac{1}{2}(-i\epsilon + \sqrt{4\alpha^2 + 4\beta^2 - \epsilon^2}), \end{aligned} \tag{A15}$$

and the associated (unnormalized) eigenvectors projected onto the zero-order basis are

$$\begin{bmatrix} \langle 0|\phi_1\rangle \\ \langle S|\phi_1\rangle \\ \langle A|\phi_1\rangle \end{bmatrix} = \begin{bmatrix} 0 \\ -\beta/\alpha \\ 1 \end{bmatrix}, \tag{A16}$$

$$\begin{bmatrix} \langle 0|\phi_2\rangle \\ \langle S|\phi_2\rangle \\ \langle A|\phi_2\rangle \end{bmatrix} = \begin{bmatrix} \frac{-i\epsilon - \sqrt{4\alpha^2+4\beta^2-\epsilon^2}}{2\beta} \\ \alpha/\beta \\ 1 \end{bmatrix}, \tag{A17}$$

and

$$\begin{bmatrix} \langle 0|\phi_3\rangle \\ \langle S|\phi_3\rangle \\ \langle A|\phi_3\rangle \end{bmatrix} = \begin{bmatrix} \frac{-i\epsilon + \sqrt{4\alpha^2+4\beta^2-\epsilon^2}}{2\beta} \\ \alpha/\beta \\ 1 \end{bmatrix}. \tag{A18}$$

The propagator may then be written as

$$\exp(-i\hat{W}t) = \sum_k |\phi_k\rangle \langle\phi_k^*| \exp(-iw_k t)/n_k, \tag{A19}$$

where

$$n_k = \langle\phi_k^*|\phi_k\rangle = \sum_{j=0,S,A} \langle j|\phi_k\rangle^2 . \tag{A20}$$

The bra vectors we employ, $\langle c|$ (as is most common), are defined to be the transpose of the complex conjugates of the coefficients representing their corresponding kets, $|c\rangle$. Thus $\langle c|d\rangle = \sum_j c_j^* d_j$, where $c_j = \langle j|c\rangle$, $d_j = \langle j|d\rangle$. An expression such as (A20), which involves an additional complex conjugate in the argument of the bra vector, implies that n_k is the sum of the (complex) squares of the components of $|\phi_k\rangle$, as opposed to being the more familiar sum of the squares of the magnitudes of the components. This necessary peculiarity arises from **W** being symmetric but not Hermitian. (In particular the symmetry of **W** implies for eigenvalues $w_a \neq w_b$ that $\langle\phi_a^*|\phi_b\rangle = 0$, which ultimately leads to an expression for the unity operator involving a sum of $|\phi_k\rangle \langle\phi_k^*|$ terms instead of the more familiar sum of $|\phi_k\rangle \langle\phi_k|$ terms.)

We note that for $\epsilon = \gamma_s/2 > 0$, w_2 and w_3 *always* have negative imaginary components. As $t \to \infty$, only the $k = 1$ contribution to (A19) survives because only w_1 has no decay (or negative imaginary) component. If we initiate the system with one QD excited, then

$$\begin{bmatrix} a_0(0) \\ a_S(0) \\ a_A(0) \end{bmatrix} = \begin{bmatrix} 0 \\ \frac{1}{\sqrt{2}} \\ \frac{1}{\sqrt{2}} \end{bmatrix}. \tag{A21}$$

The asymptotic amplitude for a_S is then

$$\begin{aligned} a_S(\infty) &= \langle S|\Psi(\infty)\rangle \\ &= \langle S|\phi_1\rangle \langle \phi_1|\Psi(0)\rangle \\ &= \frac{1}{\sqrt{2}(1+x^2)} x(1-x), \end{aligned} \tag{A22}$$

where

$$x = \frac{\beta}{\alpha} = \frac{g_1 - g_2}{g_1 + g_2}, \tag{A23}$$

and we have used the fact that $n_1 = 1 + x^2$. In a similar fashion we find

$$a_A(\infty) = \frac{1}{\sqrt{2}(1+x^2)}(1-x). \tag{A24}$$

The asymptotic concurrence in this case is simply[12]

$$\begin{aligned} C(\infty) &= \mid P_A(\infty) - P_S(\infty) \mid \\ &= \Big| \, |a_A(\infty)|^2 \; - \; |a_S(\infty)|^2 \, \Big| . \end{aligned} \tag{A25}$$

Since the magnitude of x in (A23) is always less than 1 when g_1 and g_2 are positive, $P_A > P_S$, and one can ignore the outer absolute signs. The concurrence then reduces to

$$C(\infty) = \frac{1}{2(1+x^2)^2}(1-x)^2(1-x^2). \tag{A26}$$

Viewed as a function of x, the maximum of (A26) is found to be at $x = -2 + \sqrt{3}$, and corresponds to $g_2/g_1 = \sqrt{3}$, consistent with the results in the text. For this value of x, $C(\infty) \approx 0.6495$.

The three-state model above involving the states $|q_1 = 0, q_2 = 0; s = 1\rangle$, $|S; s = 0\rangle$, and $|A; s = 0\rangle$ is convenient because it led directly to simple analytical expressions for the asymptotic concurrence. However, the same result can be obtained, with a little more work, by

employing the basis $|q_1 = 0, q_2 = 0; s = 1\rangle$, $|q_1 = 0, q_2 = 1; s = 0\rangle$ and $|q_1 = 1, q_2 = 0; s = 0\rangle$. In fact this approach is advantageous because it then is easily generalizable to $N > 2$ QDs. Assume we have N QDs, with each QDk interacting only with the dissipative plasmon via a Hamiltonian coupling term $\hbar g_k$. If the basis is taken to be $|q_1 = 0, q_2 = 0, q_3 = 0, \ldots; s = 1\rangle$, $|q_1 = 1, q_2 = 0, q_3 = 0, \ldots; s = 0\rangle$, $|q_1 = 0, q_2 = 1, q_3 = 0, \ldots; s = 0\rangle$, $\ldots$, then one has an $(N+1) \times (N+1)$ Hamiltonian matrix representation $\mathbf{H} = \hbar\mathbf{W}$ with

$$\mathbf{W} = \begin{bmatrix} -i\epsilon & g_1 & g_2 & \cdots & g_N \\ g_1 & 0 & 0 & \cdots & 0 \\ g_2 & 0 & 0 & \cdots & 0 \\ \vdots & & & \ddots & \\ g_N & 0 & 0 & \cdots & 0 \end{bmatrix}. \tag{A27}$$

The characteristic equation for the eigenvalues of $\mathbf{W}$ is then $w^{N-1}(w^2 + i\epsilon w - G) = 0$, where $G = \sum_{k=1}^{N} g_k^2$. It implies that there are $N-1$ degenerate eigenvalues $w_1 = w_2 = \ldots = w_{N-1} = 0$ and two complex eigenvalues,

$$\begin{aligned} w_N &= (-i\epsilon - \sqrt{4G - \epsilon^2})/2 \\ w_{N+1} &= (-i\epsilon + \sqrt{4G - \epsilon^2})/2. \end{aligned} \tag{A28}$$

Let $\mathbf{v^k}$ denote the eigenvector corresponding to the kth eigenvalue, and let v_j^k denote the jth component of this eigenvector. One can easily see that the $k = 1, 2, \ldots, N-1$ degenerate eigenvectors must all have $v_1^k = 0$; that is, they contain no component in the basis state $|q_1 = 0, q_2 = 0, \ldots; s = 1\rangle$. The remaining components must satisfy

$$\sum_{j=2}^{N+1} g_{j-1} v_j^k = 0. \tag{A29}$$

Although one can easily solve (A29) for low N in various ways, a systematic procedure for obtaining $N-1$ linearly independent and orthogonal eigenvectors is as follows. Notice that (A29) implies that each of the desired vectors $\mathbf{v^k}$ must be orthogonal to the vector $\mathbf{g} = (\mathbf{0}, \mathbf{g_1}, \ldots, \mathbf{g_N})^{\mathbf{T}}$. Thus one can initially set $N-1$ vectors with random coefficients and use a Gram-Schmidt procedure initiated with the vector $\mathbf{g}$, orthogonalizing all subsequent vectors against $\mathbf{g}$ and previously generated vectors.

The final two eigenvectors for $k = N$ and $k = N+1$ are easily found to have the $j = 1$ components $v_1^N = w_N/g_N$ and $v_1^{N+1} = w_{N+1}/g_N$. Their $j = 2, \ldots, N$ components

are $v_j^N = v_j^{N+1} = g_{j-1}/g_N$ and, finally, for the $j = N+1$ components, $v_{N+1}^N = v_{N+1}^{N+1} = 1$. These two eigenvectors are orthogonal to each other and the previous $N-1$ eigenvectors associated with the degenerate eigenvalue, and we find it convenient to employ them in this way with normalization considerations entering into the propagator representation, (A19).

With the systematic procedure above for evaluating all the eigenvectors, and introducing the amplitudes $b_j(t)$ corresponding to states $j = 1, 2, \ldots, N+1$ within the basis $|0,0,0,0,\ldots;1\rangle$, $|0,1,0,0,\ldots;0\rangle$, $\ldots$, $|0,\ldots,0,1;0\rangle$, one can use (A19) (extended to $N+1$ states, of course) to show

$$b_j(t) = \sum_{k=1}^{N+1} \exp(-iw_k t) K_{j,k}, \tag{A30}$$

where

$$K_{j,k} = \sum_i v_j^k v_i^k b_i(0)/n_k. \tag{A31}$$

The probabilities for QDs $1, 2, \ldots, N$ to be excited are $P_1 = \|b_2\|^2$, $P_2 = \|b_3\|^2$, $\ldots$, $P_N = \|b_{N+1}\|^2$. While obtaining bipartite concurrences may appear arduous, if $b_1(0) = 0$ (i.e., no amplitude in the state corresponds to the plasmon excited with all QDs cold) and all the other amplitudes are real, one can show that the bipartite concurrences are simply $C_{i,j} = 2\sqrt{P_i P_j}$. As with the three-state example, we note that as $t \to \infty$, only the $k = 1, 2, \ldots, N-1$ eigenvector contributions survive and one could use (A30), setting the exponential to one and carrying the sum out to only $k = N-1$, to evaluate the asymptotic populations.

Appendix B: Local Field Enhancement

To estimate Rabi-flop frequencies for the QDs, we need an estimate of the local electromagnetic field they experience, which is enhanced relative to the incident field due to the presence of the plasmonic system. To this end, we consider the interaction of one QD with a plasmonic system and employ a classical coupled dipole picture, as in Ref. 3 and associated supplementary material. The time-dependent dipoles for the plasmon ($\mu_s(t)$) and QD ($\mu_q(t)$), in the presence of an incident field with frequency ω satisfy the equations of motion

$$\ddot{\mu}_s(t) + \omega_s^2 \mu_s(t) + \gamma_s \dot{\mu}_s(t) = A_s[E_0 \cos\omega t + \mu_q(t) J] \tag{B1}$$

$$\ddot{\mu}_q(t) + \omega_q^2 \mu_q(t) + \gamma_q \dot{\mu}_s(t) = A_q[E_0 \cos\omega t + \mu_s(t) J]. \tag{B2}$$

The parameters ω_s, ω_q, and γ_s are the same as those in the CQED model of Sec. II. The other parameters in these classical equations are related to those in the CQED model as follows:

$$\begin{aligned} J &= \frac{\hbar g}{d_s d_q} \\ A_s &= 2d_s^2\omega_s/\hbar \\ A_q &= 2d_q^2\omega_q/\hbar \\ \gamma_q &= 2\gamma_d. \end{aligned} \tag{B3}$$

Several comments are in order regarding these relations. The relation for J was derived in Ref. 3. The relations for A_s and A_q reflect exactly solving (B1) and (B2) in the limit of the dipoles not interacting ($J = 0$) and equating the resulting amplitudes of oscillation of the dipoles with the corresponding quantum expressions (in the linear or low E_0 limit). These expressions are twice as small as the previously inferred ones, which were less accurate because they were based on an approximate solution of the classical equations. The classical decay factor γ_q is taken to be twice the corresponding quantum dephasing factor, γ_d. This ensures that the full-width-at-half-maximum of the isolated QD spectrum, inferred from the classical expression with γ_q, is equal to the corresponding quantum result in the low E_0 limit.

We can identify the term $\mu_s(t)J$ in (B2) as the local electric field the QD experiences because of the plasmon, that is,

$$E^{loc}(t) = \mu_s(t)J. \tag{B4}$$

For estimating E^{loc}, one can approximate $\mu_s(t)$ by the expression that results from the exact solution of (B1) in the uncoupled ($J = 0$) and on resonance ($\omega = \omega_s$) limits. This solution is readily obtained by complexifying the equation, that is, by replacing $\cos(\omega t)$ by $\exp(-i\omega t)$, which leads to an equation that is easy to solve exactly. The real part of the complex solution then solves the original, real equation. Thus,

$$\mu_s(t) \approx \frac{A_s E_0}{\omega_s \gamma_s} \sin(\omega t). \tag{B5}$$

Insertion of (B5) into (B4) leads to

$$E^{\mathrm{loc}}(t) \approx E_0^{\mathrm{loc}} \sin(\omega t), \tag{B6}$$

where

$$E_0^{\mathrm{loc}} = 2\frac{d_s}{d_q}\frac{g}{\gamma_s}E_0, \tag{B7}$$

where the expressions in (B3) have also been used.

---

[1] W. Zhang, A. O. Govorov, and G. W. Bryant, Phys. Rev. Lett. **97**, 146804 (2006).

[2] A. Ridolfo, O. Di Stefano, N. Fina, R. Saija, and S. Savasta, Phys. Rev. Lett. **105**, 263601 (2010).

[3] R. A. Shah, N. F. Scherer, M. Pelton, and S. K. Gray, Phys. Rev. B **88**, 075411 (2013).

[4] T. Hartsfield, W.-S. Chang, S.-C. Yang, T. Ma, J. Shi, L. Sun, G. Shvets, S.Link, and X. Li, PNAS **112**, 12288 (2015).

[5] W. Zhou, M. Dridi, J. Y. Suh, C. H. Kim, D. T. Co, M. R. Wasielewski, G. C. Schatz, and T. W. Odom, Nature Nanotechnology **8**, 506 (2013).

[6] C. K. Dass, T. Jarvis, V. P. Kunets, Y. I. Mazur, G. G. Salamo, C. Lienau, P. Vasa, and X. Li, ACS Photonics **2**, 1341 (2015).

[7] M. S. Tame et al., Nature Physics **9**, 329 (2013).

[8] J. F. Poyatos et al., Phys. Rev. Lett. **77**, 4728 (1996).

[9] Y. Lin et al., Nature **504**, 415 (2013).

[10] H. Krauter et al., Phys. Rev. Lett. **107**, 080503 (2011).

[11] A. Gonzalez-Tudela, D. Martin-Cano, E. Moreno, L. Martin-Moreno, C. Tejedor, and F. J. Garcia-Vidal, Phys. Rev. Lett. **106**, 020501 (2011).

[12] D. Martin-Cano, A. Gonzalez-Tudela, L. Martin-Moreno, F. J. Garcia-Vidal, C. Tejedor, and E. Moreno, Phys. Rev. B **84**, 235306 (2011).

[13] Y. He and K.-D. Zhu, Nanoscale Res. Lett. **7**, 95 (2012).

[14] Y. He and K.-D. Zhu, Quant. Info. Comp. **13**, 0324 (2013).

[15] C. Gonzalez-Ballestero et al., New J. Phys. **15**, 073015 (2013).

[16] C. Lee, New J. Phys. **15**, 083017 (2013).

[17] R. D. Artuso and G. W. Bryant, Phys. Rev. B **87**, 125423 (2013).

[18] M. Otten, R. A. Shah, N. F. Scherer, M. Min, M. Pelton, and S. K. Gray, Phys. Rev. B **92**, 125432 (2015).

[19] W. K. Wootters, Phys. Rev. Lett. **80**, 2245 (1998).

[20] J. Larson and S. M. Wild, Optim. Eng. **17**, 205 (2016).

[21] J. Larson and S. M. Wild, Preprint ANL/MCS-P5575-0316, Argonne National Laboratory, MCS

Div. (2016).

[22] S. M. Wild, Preprint ANL/MCS-P5120-0414, Argonne National Laboratory, MCS Div. (2014).

[23] S. M. Wild, J. Sarich, and N. Schunck, J. Phys. G **42**, 034031 (2015).

[24] X. Wu, S. K. Gray, and M. Pelton, Opt. Express **18**, 23633 (2010).

[25] M. Min and P. Fischer, J. Sci. Compt. **57**, 582 (2013).

[26] K. Uga, M. Min, T. Lee, and P. Fischer, Computers & Mathematics with Applications **65**, 239 (2013).

[27] W. Dür, G. Vidal, and J. I. Cirac, Phys. Rev. A **62**, 062314 (2000).

[28] J. S. Kim, A. Das, and B. C. Sanders, Phys. Rev. A **79**, 012329 (2009).

[29] H. J. Briegel and R. Raussendorf, Phys. Rev. Lett. **86**, 910 (2001).

[30] B. A. Bell, M. S. Tame, A. S. Clark, R. W. Nock, W. J. Wadsworth, and J. G. Rarity, New Journal of Physics **15**, 053030 (2013).

The submitted manuscript has been created by UChicago Argonne, LLC, Operator of Argonne National Laboratory ("Argonne"). Argonne, a U.S. Department of Energy Office of Science laboratory, is operated under Contract No. DE-AC02-06CH11357. The U.S. Government retains for itself, and others acting on its behalf, a paid-up, nonexclusive, irrevocable worldwide license in said article to reproduce, prepare derivative works, distribute copies to the public, and perform publicly and display publicly, by or on behalf of the Government.